MEDWIN PUBLISHERS
Committed to Create Value for Researchers

Nanomedicine & Nanotechnology Open Access
ISSN: 2574-187X

A Brief Overview of the Morphological Characteristics of Cain2s4-based Photocatalysts and Their Influence on Boosting the Photocatalytic Behavior

Jabbar ZH[1]*, Graimed BH[2], Al-Khayfawee AAG[3], Ammar SH[4,5] and Taofeeq H[4,6,7]

[1]Building and Construction Techniques Engineering Department, Al-Mustaqbal University College, Iraq

[2]Environmental Engineering Department, University of Baghdad, Iraq

[3]Iraqi Ministry of Health, Al-Diwaniya Teaching Hospital, Iraq

[4]Department of Chemical Engineering, Al-Nahrain University, Iraq

[5]College of Engineering, University of Warith Al-Anbiyaa, Iraq

[6]Department of Chemical and Biochemical Engineering, Missouri University of Science and Technology, USA

[7]Bipin Doshi Department of Chemical and Biochemical Engineering, Missouri University of Science and Technology, USA

***Corresponding author:** Zaid H Jabbar, Building and Construction Techniques Engineering Department, Al-Mustaqbal University College, 51001 Hillah, Babylon, Iraq, Tel: 9647830410786; Email: z.jabbar1011@coeng.uobaghdad.edu.iq

Review Article

Volume 9 Issue 2

Received Date: March 22, 2024

Published Date: April 02, 2024

DOI: 10.23880/nnoa-16000303

Abstract

CaIn2S4-based heterojunctions have gained significant attention as robust photocatalysts for sustainable environmental applications like organic degradation and H_2 production. This study introduces a brief overview of the morphological characteristics of CaIn2S4-based composites and their effects on their catalytic properties. The fabrication of CaIn2S4-based photocatalysts with hierarchical or nanosheet heterostructures could offer an adequate surface area to volume ratio, enhancing the accessibility of pollutants to the catalyst surface and boosting the photodegradation performance. Moreover, the increased active sites reflect positive effects on the visible-light absorption efficiency. The perfect interfacial contact in the CaIn2S4-based composites facilitated the photocarrier transfer, hampered their reunion rate, prolonged their lifetime, and improved their utilization. The morphological durability and stability of CaIn2S4-based composites are also important variables influencing the photoreaction capacity. Finally, the optimization of surface states and morphological defects can modify the electronic structure of CaIn2S4-based semiconductors, improving their optical properties.

Keywords: CaIn2S4-Based Composites; Morphological Characteristics; Photocatalytic Reaction; Charge Separation Performance

Abbreviations: SPR: Surface Plasmon Resonance; TEM: Transmission Electron Microscopy; ITO: Conductive Glass Substrates; SEM: Scanning Electron Microscope; TRPL: Time Resolved Photoluminescence Spectra; MO: Methyl Orange; XRD: X-Ray Diffraction; FTIR Fourier-Transform Infrared Spectroscopy; NPs: Nanoparticles; XPS X-Ray Photoelectron Spectroscopy; DFT: Density Functional Theory; SAED: Selected Area Electron Diffraction; BET: Brunauere-

Emmette-Teller; TPR: Transient Photocurrent Response; EIS: Electrochemical Impedance Spectroscopy; IEF: Internal Electric Field.

Introduction

The photocatalysis process has emerged as an attractive option to solve the challenges related to the energy crisis, offering the opportunity to harvest renewable solar energy for environmental applications and energy conversion [1-6]. In recent years, various types of ternary metal sulfides like $MgIn_2S_4$ [7,8], $ZnIn_2S_4$ [9,10], $CaIn_2S_4$ [11,12], and $CdIn_2S_4$ [13,14] have been significantly employed for photocatalytic purposes due to their strong visible-light utilization capacity. In particular, typical ternary sulfide-based semiconductors have been considered efficient photocatalysts owing to their excellent light absorption activity, high stability, good catalytic activity, narrow band gap, and appropriate morphology [15,16]. Unfortunately, the poor surface area, the rapid charge annihilation efficiency, and the intrinsic photocarrier characteristics obstruct further advancement of the pure $CaIn_2S_4$ photocatalysts [17].

In this regard, the construction of $CaIn_2S_4$-based heterojunctions and modification of their morphologies can be considered a rich strategy for improving the photocatalytic properties, such as stability and durability, visible-light absorption efficiency, charge carrier dynamics, and specific surface area [18,19]. It was reported that the doping of hierarchical $CaIn_2S_4$ with bimetallic Au-Pt alloy nanoparticles can promote the solar-light harvesting of $CaIn_2S_4$-based heterojunction. The expanded absorption activity was linked to the strong surface plasmon resonance (SPR) behavior of Au particles and the scattering effect of Pt particles. Besides, the interaction of metal- support exhibited a prominent impact on the morphology of incorporated metals. The poor cooperation between $CaIn_2S_4$ and Au produces larger sizes and well-organized structures, while the strong connection between $CaIn_2S_4$ and Au results in smaller sizes and disorganized structures [20]. Zhang W, et al. [21] declared that the morphological modification of $CaIn_2S_4$-based photocatalysts by loading hierarchical $CaIn_2S_4$ films onto conductive glass substrates (ITO) enhanced the photocatalytic stability via three cycles of methyl orange (MO) degradation. Furthermore, it was detected that the construction of $CaIn_2S_4$-based heterojunction with flower-like/flower-like morphology recorded upgraded Cr(VI) reduction. The enhanced charge reunion efficiency of type II $CaIn_2S_4/ZnIn_2S_4$ heterojunction was mainly behind the improved photocatalytic activity [22].

This review introduces a comprehensive yet concise overview of the morphological characteristics of $CaIn_2S_4$-based photocatalysts and their pivotal role in enhancing the photocatalytic behavior. By collecting all the latest work dealing with $CaIn_2S_4$-based photocatalysts, our study offers key advancements in synthesis strategies and structural and morphological characterization techniques. This argument also discusses the influence of morphological characteristics of $CaIn_2S_4$-based photocatalysts on their catalytic properties, like pollutant degradation, solar-light response, charge separation, photostability, and surface area. In other words, our overview focuses on the intricate interplay between the morphology of $CaIn_2S_4$-based and photocatalytic activity, supported by sophisticated characterization technologies like SEM, TEM, HRTEM, EDS, XRD, FTIR, XPS, PL, TRPL, EIS, DRS, and DFT calculations. Finally, our work may help the researchers design and develop robust $CaIn_2S_4$-based heterojunctions with desirable morphology and catalytic capacity.

Fabrication of $CaIn_2S_4$-Based Nanomaterials

Nanomaterials have introduced significant efforts in developing the field of photocatalysis due to their unique properties that result from their large surface area-to-volume ratio, providing numerous active sites, enhancing light absorption, accelerating charge mobility, and promoting pollutant selectivity. The nanomaterials recorded crucial significance in medical applications, such as tissue engineering scaffolds, imaging agents for diagnostics, and targeted drug delivery. The small size and high surface area of nanomaterials enable precise drug targeting, which minimizes side effects. Furthermore, these materials enhance contrast in medical imaging and provide structural support for regenerative medicine approaches, advancing treatment options for various diseases. Besides, nanomaterials were intensively employed in many environmental applications and energy conversions, such as organic degradation, CO_2 conversion, hydrogen production, and solar cells. In the catalytic sector, nano-photocatalysts offer plenty of active sites and upgrade the adsorption and photoreaction kinetics, resulting in improved pollutant degradation processes. The researchers manifested various outstanding technologies for the synthesis of nanomaterials, like hydrothermal, solvothermal, sol-gel, co-precipitation, and so on [23-27].

Among them, the hydrothermal strategy is considered the main and most facile method to fabricate pure $CaIn_2S_4$ (CIS) photocatalysts. In brief, 8 mmol of thioacetamide, 4 mmol of $In(NO_3)3•4.5H_2O$ and 2 mmol of $CaCl_2•2H_2O$ were dissolved in 30 mL of ethanol and 30 mL of deionized water with continuous stirring for 30 min. After that, the mixture was thermally reacted via a 100 mL Teflon-lined-stainless-steel autoclave at 120 °C for 24 h to produce a flower-like $CaIn_2S_4$ microsphere. As shown in Figure 1, the same steps were employed to fabricate $Co_3O_4/CaIn_2S_4$ after the addition of Co_3O_4 nanoparticles, exhibiting strong interconnection

between Co_3O_4 and $CaIn_2S_4$ [28]. Moreover, Yuan W, et al. [29] revealed the fabrication of $CaIn_2S_4$ nanosheets via modifying the synthesis procedure above by raising the reaction autoclave temperature to 160 °C and reducing the reaction period to 24 h. In another work, very thin $CaIn_2S_4$ nanoparticles decorated RGO sheets were fabricated using the hydrothermal method by extending the reaction time to 24 h.

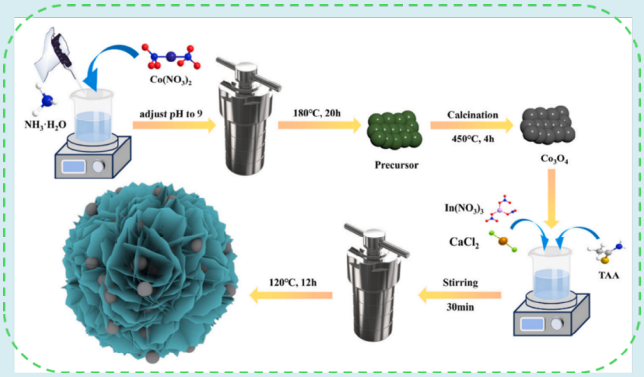

Figure 1: Synthesis procedure of $Co_3O_4/CaIn_2S_4$ heterojunction via hydrothermal method [28].

Crystal Structure of $CaIn_2S_4$-based

Different powerful and sophisticated technologies were employed to characterize $CaIn_2S_4$-based photocatalysts. The crystal structure of $CaIn_2S_4$-based photocatalysts was perfectly identified by X-ray diffraction (XRD). For instance, Zhang P, et al. [30] introduced the XRD patterns of $CaIn_2S_4/TiO_2$ composites. As revealed in Figure 1a, the $CaIn_2S_4/TiO_2$ recorded some XRD peaks at 27.43° (311), 33.40° (400), and 47.90° (440), which belonged to cubic $CaIn_2S_4$ (JCPDS no. 31–0272), while the other peaks were attributed to crystal planes of anatase TiO_2 (JCPDS no. 21–1272). This implies the good crystallinity and high phase purity of $CaIn_2S_4/TiO_2$ composites. The functional group and composition of $CaIn_2S_4$-based hybrids can be identified via Fourier-transform infrared spectroscopy (FTIR). Figure 2b depicts the FTIR spectra of $ZnIn_2S_4/Er^{3+}:Y_3Al_5O_{12}@ZnTiO_3/CaIn_2S_4$. The FTIR signals at 681.27 cm^{-1}, 599.98 cm^{-1}, 583.98 cm^{-1}, 557.5 cm^{-1}, and 455.52 cm^{-1}, which consistent with the stretching vibrations Ca-S, In-S, Zn-S, Ti-O, Zn-O in $CaIn_2S_4$, $ZnIn_2S_4$, $ZnTiO_3$, respectively, verifying the perfect composition of $ZnIn_2S_4/Er^{3+}:Y_3Al_5O_{12}@ZnTiO_3/CaIn_2S_4$ [19].

Besides, the chemical state and the charge transfer of $CaIn_2S_4$-based heterojunctions can be demonstrated via X-ray photoelectron spectroscopy (XPS). For example, the XPS survey of $CaIn_2S_4$/BiOCl-SOVs revealed the presence of S, In, Ca, Cl, O, and Bi in the $CaIn_2S_4$/BiOCl-SOVs composite (Figure 2c). In addition, the high-resolution Ca 2p peaks at 347.26 eV and 351.03 eV belonged to Ca $2p_{1/2}$ and Ca $2p_{3/2}$ in Ca^{2+} (Figure 2d). As revealed in Figure 2e, the in 3d signals at 452.09 eV and 444.53 eV were in accordance with in $3d_{3/2}$ and In $3d_{5/2}$, respectively. Furthermore, the XPS peaks of S 2P were not observed due to the overlapping with Bi 4f peaks (Figure 2f). Importantly (Figures 2g-2i), the positive shifting in binding energies of pure BiOCl (Bi 4f, Cl 2p, and O 1s) compared with $CaIn_2S_4$/BiOCl-SOVs demonstrates the electron transfer from $CaIn_2S_4$ to BiOCl, creating S-scheme heterojunction system [31].

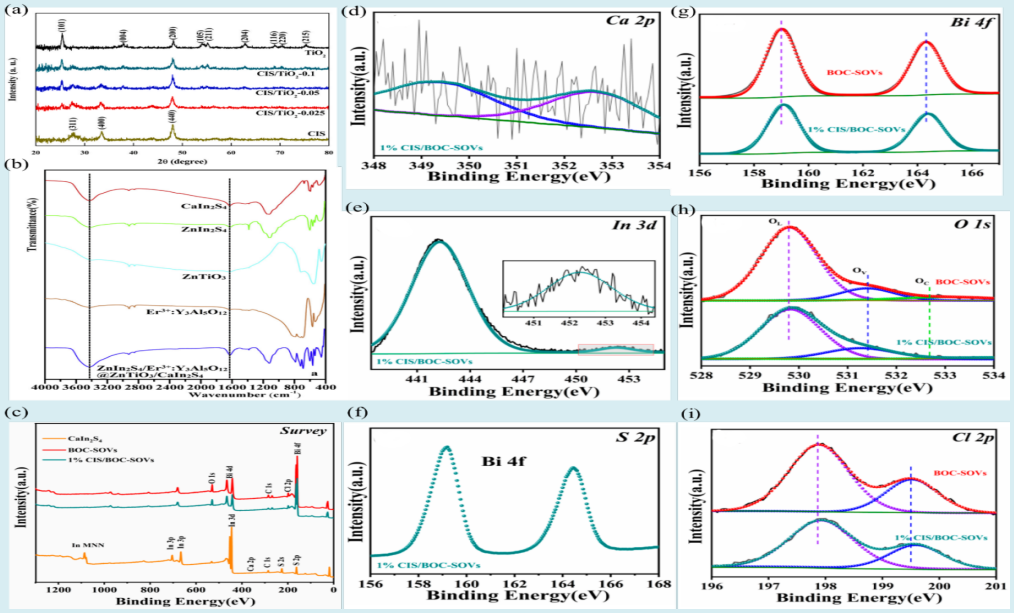

Figure 2: (a) XRD patterns of $CaIn_2S_4/TiO_2$ [30], (b) $ZnIn_2S_4/Er3+:Y_3Al_5O_{12}@ZnTiO_3/CaIn_2S_4$ [19], (c-i) XPS spectra of the $CaIn_2S_4$/BiOCl-SOVs composite [31].

Morphology of $CaIn_2S_4$-based Heterojunctions

Understanding and optimizing the $CaIn_2S_4$-based structure is important to developing powerful $CaIn_2S_4$-based heterojunctions for environmental applications. In general, the pure $CaIn_2S_4$ photocatalyst can be fabricated in 2D structures (nanosheets, nanoplates, and nanoflakes) and 3D morphology (microsphere or flower-like structure). These morphologies enable the $CaIn_2S_4$ catalyst to provide an immobilizing framework for other co-catalysts, creating an efficient $CaIn_2S_4$-based heterojunction with favorable surface area, strong interfacial contact, excellent charge transfer efficiency, and robust stability [20,30,32-34]. For instance, the morphologies of $SrTiO_3/CaIn_2S_4$ were analyzed via scanning electron microscope (SEM) technology. For Figure 3a, the pure $CaIn_2S_4$ revealed a micro-sphere shape composed of self-assembled nanosheets. According to Figure 3b, the pure $SrTiO_3$ catalyst appeared to have a particle-like morphology with diameters around 150–200 nm. Obviously, the $SrTiO_3/CaIn_2S_4$ composites introduced a flower-like structure loaded with $SrTiO_3$ particles, forming a stable heterojunction system (Figure 3c). The intimate contact in the interfaces facilitates the charge transfer between $SrTiO_3$ and $CaIn_2S_4$, constructing an S-scheme heterojunction system (Figure 3d) [35].

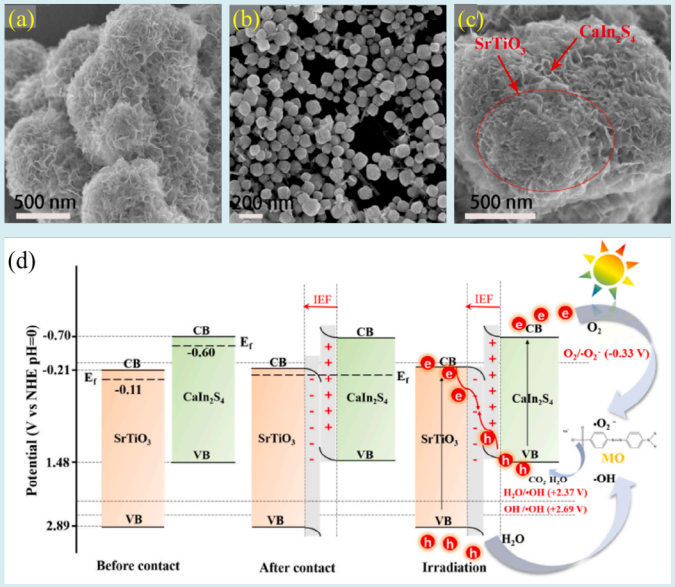

Figure 3: (a-c) SEM images of $CaIn_2S_4$, $SrTiO_3$, and $SrTiO_3/CaIn_2S_4$ respectively, (d) S-scheme charge transfer route in the $SrTiO_3/CaIn_2S_4$ heterojunction [35].

Transmission electron microscopy (TEM) provides crucial details about the microstructural features of $CaIn_2S_4$-based heterojunctions. Bariki R, et al. [36] reported UiO-66(–NH_2)/$CdIn_2S_4$/$CaIn_2S_4$ heterostructure (UN/CDS/CAS) for efficient asulam degradation and H_2 production. For Figure 4a & 4b, the TEM images present the epitaxial growth of ultra-thin $CaIn_2S_4$ nanosheets and UiO-66(–NH2) nanospecies onto the 3D hierarchical $CdIn_2S_4$ nanorods. As exhibited in Figure 4c, the high-resolution TEM (HRTEM) displayed three lattice spacings at 0.32 nm, 0.265 nm, and 0.195 nm. The first two lattice fringes were in accordance with the (311) and (400) planes of $CdIn_2S_4$, and the last one belonged to the (440) plane of cubic $CaIn_2S_4$. The presence of $CdIn_2S_4$ and $CaIn_2S_4$ could be further verified by selected area electron diffraction (SAED). The SAED pattern depicted the same d-spacing values as HRTEM, confirming the powerful hybridization of composite semiconductors (Figure 4d). The real heterojunction among three catalysts generates an internal electric field (IEF) at their interfaces, encouraging the recombination between the feeble electrons in the valence band (VB) of UiO-66(–NH_2) and the weak holes in the conduction band (CB) of $CdIn_2S_4$ and $CaIn_2S_4$, forming boosted dual S-scheme charge transfer pathways (Figure 4e).

In another work, the TEM and HRTEM images in Figures 5a-5c showed the formation of pristine $CaIn_2S_4$ with lattice spacings at 0.27 nm (400). After immobilization of CoS_2, the $CaIn_2S_4$ nanosheets were assembled and displayed flower-like morphology to support CoS_2 NPs (Figure 5d-5f). Moreover, the elemental mapping images of $CoS_2/CaIn_2S_4$ displayed the well distribution of Co, S, In, and Ca elements in the binary catalyst, proving the probability of constructing interfacial heterojunction between the two catalysts (Figures 5g-5k). Brunauere-Emmette-Teller (BET) analysis revealed that these regular depositions of CoS_2 NPs can significantly influence the texture properties of $CaIn_2S_4$. As shown in

Figure 6a, the pure CoS_2 nanoparticles exhibited a type III isotherm, which indicates their weak interactions with nitrogen molecules. After dispersing the CoS_2 nanoparticles onto $CaIn_2S_4$ nanosheets, the $CoS_2/CaIn_2S_4$ composite manifested type IV with a mesoporous texture (Figure 6b). Besides, the introduction of CoS_2 NPs amazingly improved the surface area of $CaIn_2S_4$ from 4.08 to 72.63 m2/g [37]. The stronger surface area provides more active sites for adsorption and photoreaction, thereby upgrading catalytic performance [38,39].

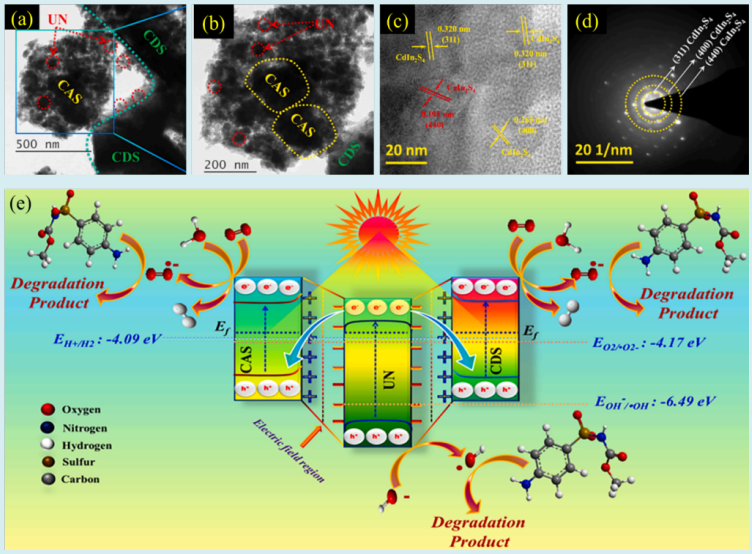

Figure 4: (a-b) TEM images, (c) HRTEM images, (d) SAED pattern, and (e) dual S-scheme mechanism of the ternary UiO-66(–NH_2)/$CdIn_2S_4$/$CaIn_2S_4$ heterojunction [36].

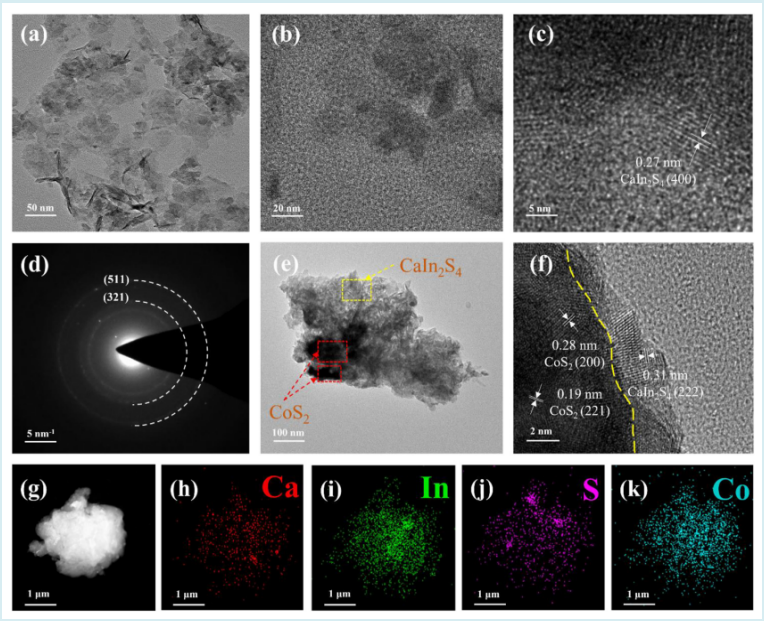

Figure 5: (a-c) TEM and HRTEM images of pure $CaIn_2S_4$, (d-f) SAED, TEM, and HRTEM images of the $CoS_2/CaIn_2S_4$ composite, (g-k) Elemental mapping of the $CoS_2/CaIn_2S_4$ hybrid [37].

Furthermore, it was discovered that the random scattering of CeO_2 NPs onto hierarchical $CaIn_2S_4$ could increase the BET surface area from 72.75 m^2/g to 75.93 m^2/g (Figure 6c). This implies that the hybridization of CeO_2 NPs with $CaIn_2S_4$ can provide excessive active sites to upgrade the photocatalytic degradation performance [40]. On the other hand, the combination of the $CaIn_2S_4$ catalyst with other photocatalysts or plasmonic metal NPs can create synergistic

efforts, further enhancing the catalytic performance. In other words, the hierarchical and nanosheet morphologies supplied appropriate effective sites to incorporate with other co-catalysts, resulting in improved degradation performance, charge separation efficiency, stability, light harvesting activity, stability and recyclability, and mass transfer and reactant accessibility [41,42]. For example, Li J, et al. [43] demonstrated that the interfacial contact between the plasmonic Au NPs and $CaIn_2S_4$ nanosheets could enhance the methylene blue degradation rate and electron transfer from Au NPs to $CaIn_2S_4$ by surface plasmon resonance (SPR) effect (Figure 6d-6f).

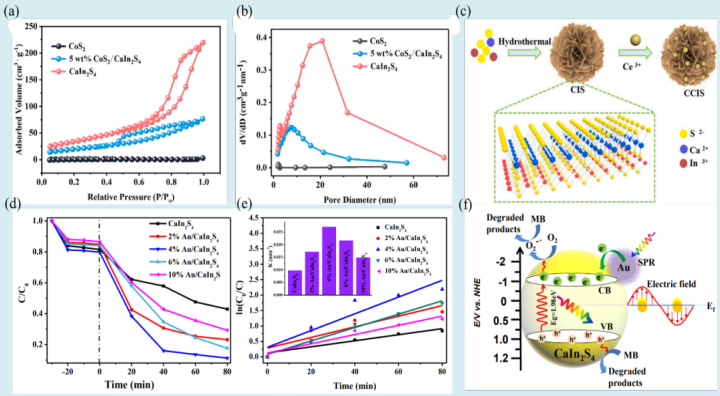

Figure 6: (a-b) Nitrogen adsorption isotherm and pore size distribution of the $CoS_2/CaIn_2S_4$ composite [37], (c) structure of the $CeO_2/CaIn_2S_4$ composite [40], (d-e) photocatalytic performance, degradation kinetics of plasmonic, and photocatalytic mechanism of MB degradation over Au/ $CaIn_2S_4$ composites [43].

In another investigation, the electrospinning method was employed to fabricate In_2O_3 fibers with a diameter of approximately 50 nm (Figure 7a). As illustrated in the morphological images of Figure 7b, the $CaIn_2S_4$-based nanofibers were developed by growing $CaIn_2S_4$ nanofoils onto In_2O_3 fibers to generate a type II heterojunction system. This strong interaction can stimulate charge migration and separation in the type II heterojunction. The density functional theory (DFT) was employed to identify the electronic structures of In_2O_3 and $CaIn_2S_4$ to demonstrate the boosted photocarrier separation of $CaIn_2S_4$-based nanofibers. As revealed in Figures 7c & 7d, the CBs of both semiconductors consist of In 5s orbits, while the VBs are composed of O 2p and S 2p orbits for In_2O_3 and $CaIn_2S_4$ respectively. Although their CBs originated from in atoms, the CBs have distinct band dispersions for In_2O_3 and $CaIn_2S_4$. It can be detected that photoinduced electrons in In_2O_3 revealed higher mobility than those in $CaIn_2S_4$, proving the electron drifting from In_2O_3 to $CaIn_2S_4$ in a type II heterojunction system (Figure 7e) [44].

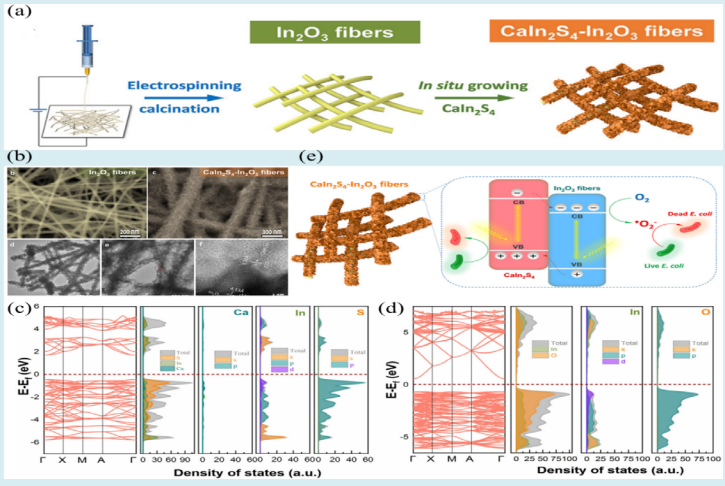

Figure 7: (a) synthesis procedure of $CaIn_2S_4$-based nanofibers, (b) SEM, TEM, and HRTEM images of $CaIn_2S_4/In_2O_3$ nanofibers, (c-d) Electronic structures of In_2O_3 and $CaIn_2S_4$ using DFT calculations, (e) type II heterojunction mechanism of $CaIn_2S_4/In_2O_3$ nanofibers [44].

The morphological features of hierarchical $CaIn_2S_4$-based photocatalysts can promote light utilization activity and scattering effects [12]. For example, diffuse reflectance spectroscopy (DRS) spectra of UiO-66(–NH_2)/$CdIn_2S_4$/$CaIn_2S_4$ (UN/CDS/CAS) hybrids recorded a dramatic shift in light utilization wavelength compared with pure samples (Figure 8a). Besides, the significant reduction in the photoluminescence (PL) spectra indicates that the hierarchical morphology can also minimize the recombination rate of UN/CDS/CAS (Figure 8b). As exhibited in Figure 8c, the time resolved photoluminescence spectra (TRPL) of UN/CDS/CAS obtained a notable reduction in PL lifetime, recording rapid separation of photocarriers in the flower-like UN/CDS/CAS structure [36]. In another example, the transient photocurrent response (TPR) of $CaIn_2S_4$/BiOCl-SOVs offered the strongest TPR emission, indicating that the hierarchical structure facilitates charge carrier separation (Figure 8d). Furthermore, electrochemical impedance spectroscopy (EIS) of the same composite showed the smallest arc radius, implying the limited interfacial resistance of the photocarrier in the $CaIn_2S_4$/BiOCl-SOVs hybrid (Figure 8e) [31].

Morphological photostability and structure durability are also additional key parameters that influence catalytic activity. Efficiently constructed hierarchical and nanosheet structures can introduce enhanced durability under photodegradation reactions and enable simple recycling of the catalyst for multiple photoreaction cycles [15]. Gao X, et al. [45] stated that the hierarchical $CaIn_2S_4$ can act as a robust immobilizing framework for Sr-SnS_2, which reflected excellent stability and reusability in five successive recycling of reduction Cr(VI) (Figure 8f). Furthermore, the authors revealed that the perfect combination of two morphologies can stimulate photocarrier migration in the S-scheme pathways (Figure 8g). In addition, the 3D charge density difference was provided to further investigate the distribution of photocarriers at the interfaces of hierarchical $CaIn_2S_4$/Sr-SnS_2. As revealed in Figure 8h, the blue area depicts the electron consumption on the surface of Sr-SnS_2, while the yellow area indicates the electron accumulation on the surface of $CaIn_2S_4$, which suggests the establishment of IEF between $CaIn_2S_4$ and Sr-SnS_2, improving the S-scheme mechanism.

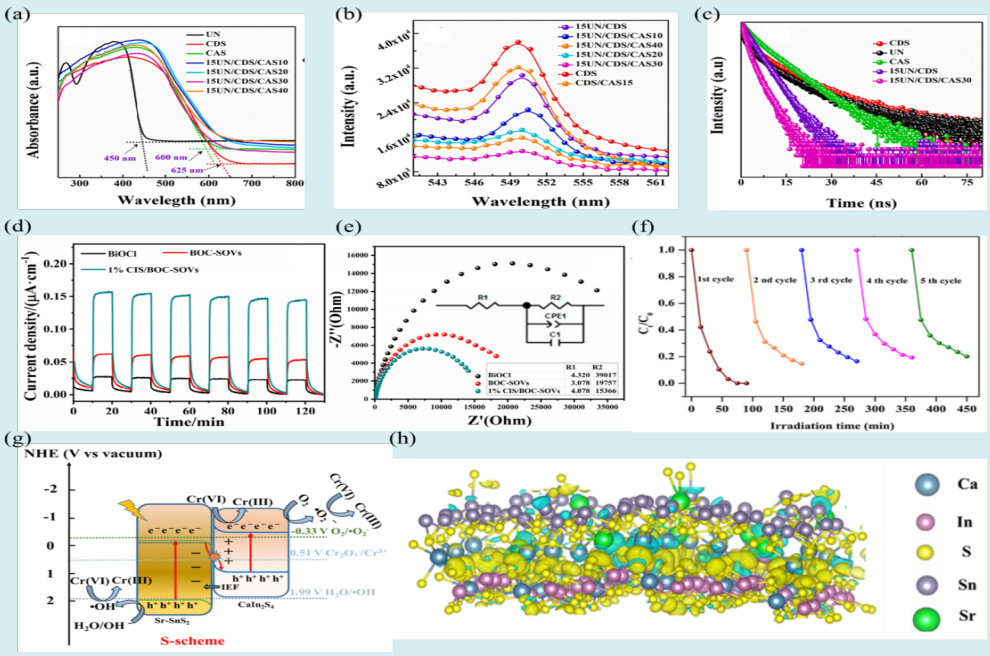

Figure 8: (a-c) DRS, PL, and TRPL of hierarchical UN/CDS/CAS [36], (d-e) TPR and EIS spectra of flower-like $CaIn_2S_4$/BiOCl-SOVs [31], (f-h) cycling experiments, S-scheme diagram, and DFT charge difference density diagram of hierarchical $CaIn_2S_4$/Sr-SnS_2 [45].

Conclusion

This review introduces a novel discussion about the morphological influence of $CaIn_2S_4$-based heterojunctions on their catalytic properties. The hydrothermal strategy is considered the main and most facile method to fabricate pure $CaIn_2S_4$ and their composites. The crystal structure of $CaIn_2S_4$-based photocatalysts was perfectly identified by XRD, which implied the good crystallinity and high phase purity of $CaIn_2S_4$/TiO_2 composites. The functional group and

composition of $CaIn_2S_4$-based hybrids can be identified via FTIR analysis. The chemical state and the charge transfer of $CaIn_2S_4$-based heterojunctions can be demonstrated via XPS spectra. The positive and negative shifting in binding energies of pure $CaIn_2S_4$ compared with composites can give an important hint about the electron transfer in the $CaIn_2S_4$-based heterojunctions. In previous studies, the pure $CaIn_2S_4$ photocatalysts were fabricated in 2D structures (nanosheets, nanoplates, and nanoflakes) and 3D morphology (microsphere or flower-like structure). The morphological characteristics of $CaIn_2S_4$-based heterojunction can play a crucial role in improving the photocatalytic capacity by influencing factors, such as stability and durability, light harvesting efficiency, charge carrier dynamics, and specific surface area. Controlling the morphology of $CaIn_2S_4$-based heterojunctions through the synthesis procedures is helpful to optimize the catalytic capacity of $CaIn_2S_4$-based nanomaterials for various environmental applications, including energy conversion, pollutant degradation, and water splitting.

Acknowledgements

"The authors are grateful to Al-Mustaqbal University College, Building and Construction Techniques Engineering Department for their support".

References

1. Ikreedeegh RR, Hossen MA, Tahir M, Abd Aziz A (2024) A comprehensive review on anodic TiO_2 nanotube arrays (TNTAs) and their composite photocatalysts for environmental and energy applications: Fundamentals, recent advances and applications. Coord Chem Rev 499: 215495.

2. Kumar A, Rana S, Dhiman P, Sharma G, Stadler FJ (2024) Current progress in heterojunctions based on Nb_2O_5 for photocatalytic water treatment and energy applications. J Mol Liq 399: 124360.

3. Graimed BH, Jabbar ZH, Alsunbuli MM, Ammar SH, Hamood SA, et al. (2023) Rational design of 1D TaON nano-fibrous network decorated 2D BiOBr nanosheets for sustainable photocatalytic detoxification of antibiotics in wastewater via S-scheme heterostructure system. J Water Process Eng 54: 104059.

4. Jabbar ZH, Graimed BH, Ammar SH, Sabit DA, Najim AA, et al. (2024) The latest progress in the design and application of semiconductor photocatalysis systems for degradation of environmental pollutants in wastewater: Mechanism insight and theoretical calculations. Mater Sci Semicond Process 173: 108153.

5. Fu X, Huang H, Tang G, Zhang J, Sheng J, et al. (2024) Recent advances in g-C_3N_4-based direct Z-scheme photocatalysts for environmental and energy applications. Chinese J Struct Chem 100214.

6. Morshedy AS, El-Fawal EM, Zaki T, El-Zahhar AA, Alghamdi MM, et al. (2024) A review on heterogeneous photocatalytic materials: Mechanism, perspectives, and environmental and energy sustainability applications. Inorg Chem Commun pp: 112307.

7. Yu J, Yan P, Chen F, Jin S, Xu X, et al. (2023) $MgIn_2S_4$@ In_2O_3 hierarchical tubular heterostructures with expedited photocarrier separation for efficient visible-light-driven antimicrobial activity. Chem Eng J 452(4): 139559.

8. Jin H, Luo L, Naghizadeh M, Liu Q, Dong S, et al. (2023) Rapid photocatalytic reduction of hexavalent chromium over Z-scheme $MgIn_2S_4/BiPO_4$ heterojunction: Performance, DFT calculation and mechanism insight. Chemosphere 335: 139175.

9. Wang R, Yu W, Fang N, Wang P, Chu Y, et al. (2024) Constructing fast charge separation of $ZnIn_2S_4$ @$CuCo_2S_4$ p-n heterojunction for efficient photocatalytic hydrogen energy recovery from quinolone antibiotic wastewater. Appl Catal B Environ 341: 123284.

10. Liu HY, Niu CG, DHuang DW, Liang C, Guo H, et al. (2023) Unravelling the role of reactive oxygen species in ultrathin Z-scheme heterojunction with surface zinc vacancies for photocatalytic H_2O_2 generation and CTC degradation. Chem Eng J 465: 143007.

11. Ding J, Li X, Chen L, Zhang X, X Tian X (2018) Photocatalytic hydrogen production over plasmonic AuCu/$CaIn_2S_4$ composites with different AuCu atomic arrangements. Appl Catal B Environ 224: 322-329.

12. Xia Y, Li Q, Wu X, Lv K, Tang T, et al. (2017) Facile synthesis of CNTs/$CaIn_2S_4$ composites with enhanced visible-light photocatalytic performance. Appl Surf Sci 391: 565-571.

13. Ma X, Li W, Li H, Dong M, Geng L, et al. (2023) Novel noble-metal-free $Co_2P/CdIn_2S_4$ heterojunction photocatalysts for elevated photocatalytic H_2 production: Light absorption, charge separation and active site. J Colloid Interface Sci 639: 87-95.

14. Xie L, Liu G, Suo R, Xie Z, Liu H, et al. (2023) Construction of a Z-scheme $CdIn_2S_4$/ZnS heterojunction for the enhanced photocatalytic hydrogen evolution. J Alloys Compd 948: 169692.

15. Zhuge Z, Liu X, Chen T, Gong Y, Li C, et al. (2021) Highly efficient photocatalytic degradation of different

hazardous contaminants by $CaIn_2S_4$-$Ti_3C_2T_x$ Schottky heterojunction: An experimental and mechanism study. Chem Eng J 421: 127838.

16. Liu B, Liu X, Li L, Zhuge Z, Li Y, et al. (2019) $CaIn_2S_4$ decorated WS_2 hybrid for efficient Cr(VI) reduction. Appl Surf Sci 484: 300-306.

17. Ding J, Yan W, Sun S, Bao J, Gao C (2014) Hydrothermal synthesis of $CaIn_2S_4$-reduced graphene oxide nanocomposites with increased photocatalytic performance. ACS Appl Mater Interfaces 6(15): 12877-12884.

18. Wang XJ, Li XL, Liu C, Li FT, Li YP, et al. (2018) Metalloid Ni_2P and its behavior for boosting the photocatalytic hydrogen evolution of $CaIn_2S_4$. Int J Hydrogen Energy 43(1): 219-228.

19. Wang J, Wang D, Zhang X, Zhao C, Zhang M, et al. (2019) An anti-symmetric dual (ASD) Z-scheme photocatalytic system: ($ZnIn_2S_4/Er^{3+}$:$Y_3Al_5O_{12}$@$ZnTiO_3$/$CaIn_2S_4$) for organic pollutants degradation with simultaneous hydrogen evolution. Int J Hydrogen Energy 44: 6592-6607.

20. Ding J, Li X, Chen L, Zhang X, Sun S, et al. (2016) Au-Pt alloy nanoparticles site-selectively deposited on $CaIn_2S_4$ nanosteps as efficient photocatalysts for hydrogen production. J Mater Chem A 2016(32): 12630-12637.

21. Zhang W, Chen H, Zhang L, Zhang S, Dong E, et al. (2020) A facile hydrothermal approach for the deposition of $CaIn_2S_4$ hierarchical nanosheet films for photocatalytic application. J Alloys Compd 821: 153545.

22. Xu S, Dai J, Yang J, You J, Hao J (2018) Facile synthesis of novel $Cain_2S_4$/$ZnIn_2S_4$ composites with efficient performance for photocatalytic reduction of cr(VI) under simulated sunlight irradiation. Nanomaterials 8(7): 472.

23. Ahmad KP, Khan A, Abdellatif AAH, Abu-Dief AM, Al-Anzi BS, et al. (2024) Development of CuO and CuO: Zn^{2+} nano-oxides for dye degradation and pharmaceutical studies. Inorg Chem Commun 160: 111887.

24. Alahmadi M, Alsaedi WH, Mohamed WS, Hassan HMA, Ezzeldien M, et al. (2023) Development of Bi_2O_3/$MoSe_2$ mixed nanostructures for photocatalytic degradation of methylene blue dye. J Taibah Univ Sci 17(1): 2161333.

25. Alzaid M, Mohamed WS, Alanazi R, Alsohaimi IH, Hassan HMA, et al. (2023) Novel (Y_2O_3) x (CdO) $_{1-x}$ binary mixed oxide nanocomposites: facile synthesis, characterization, and photocatalysis enhancement. J Mater Res Technol 23: 2454-2466.

26. Abu-Dief AM, Essawy AA, Diab AK, Mohamed WS (2021) Facile synthesis and characterization of novel Gd_2O_3–CdO binary mixed oxide nanocomposites of highly photocatalytic activity for wastewater remediation under solar illumination. J Phys Chem Solids 148: 109666.

27. Mohamed WS, Abu-Dief AM (2018) Synthesis, characterization and photocatalysis enhancement of Eu_2O_3-ZnO mixed oxide nanoparticles. J Phys Chem Solids 116: 375–385.

28. Yan Z, Zhang X, Yu B, Yao J, Han D, et al. (2024) Integrating $CaIn_2S_4$ nanosheets with Co_3O_4 nanoparticles possessing semiconducting and electrocatalytic properties for efficient photocatalytic H2 production. Ceram Int 50(2): 3052-3063.

29. Yuan W, Yang S, Li L (2015) Synthesis of g-C_3N_4/$CaIn_2S_4$ composites with enhanced photocatalytic activity under visible light irradiation. Dalt Trans 44(36): 16091-16098.

30. Zhang P, Zhang L, Dong E, Zhang X, Zhang W, et al. (2021) Synthesis of $CaIn_2S_4$/TiO_2 heterostructures for enhanced UV–visible light photocatalytic activity. J Alloys Compd 885: 161027.

31. Zhang Z, Zhang Y, Han X, Guo L, Wang D, et al. (2021) Assembly of $Caln_2s_4$ on defect-rich biocl for acceleration of interfacial charge separation and photocatalytic phenol degradation via s-scheme electron transfer mechanism. Catalysts 11(9): 1130.

32. Sabit DA, Ebrahim SE, Jabbar ZH (2023) Immobilization of 0D CuO/$ZnFe_2O_4$ nanoparticles onto 2D BiOBr nanoplates as dual S-scheme heterostructure for boosting photocatalytic oxidation of levofloxacin in wastewater: Magnetic reusability and mechanism insights. J Photochem Photobiol A Chem 443: 114849.

33. Jabbar ZH, Graimed BH, Okab AA, Alsunbuli MM, Al-husseiny RA (2023) Construction of 3D flower-like Bi_5O_7I/Bi/Bi_2WO_6 heterostructure decorated $NiFe_2O_4$ nanoparticles for photocatalytic destruction of Levofloxacin in aqueous solution: Synergistic effect between S-scheme and SPR action. J Photochem Photobiol A Chem 441: 114734.

34. Jabbar ZH, Graimed BH, Ammar SH, Al-Jubouri SM, Abbar AH, et al. (2024) Rational design of novel 0D/0D $Bi_2Sn_2O_7$/CeO_2 in the core-shell nanostructure for boosting the photocatalytic decomposition of antibiotics in wastewater: S-type-based mechanism. Mater Sci Semicond Process 173: 108165.

35. Chen S, Chen C, Cheng C, Shu L, Tang Z, et al. (2023) Construction of $SrTiO_3/CaIn_2S_4$ S-scheme heterojunction for enhanced photocatalytic degradation of organic pollutants. Mater Sci Semicond Process 164: 107627.

36. Bariki R, Pradhan SK, Panda S, Nayak SK, Majhi D, et al. (2023) In-situ synthesis of structurally oriented hierarchical UiO-66 $(-NH_2)/CdIn_2S_4/CaIn_2S_4$ heterostructure with dual S-scheme engineering for photocatalytic renewable H2 production and asulam degradation. Sep Purif Technol 314: 123558.

37. Li J, Yu Q, Zhang X, Xiong X, Jin Y, et al. (2024) Coupling CoS_2 and $CaIn_2S_4$ for efficient electron trapping and improved surface catalysis to promote solar hydrogen evolution. Int J Hydrogen Energy 51: 314-326.

38. Mahmoud SM, Ammar SH, Ali ND, Ali FD, Jabbar ZH (2024) Visible-light-prompted photocatalytic degradation of emerging contaminants over facile constructed ZIF-67/ Bi_25FeO_40 hybrids. J Water Process Eng 59: 104990.

39. Graimed BH, Jabbar ZH, Alsunbuli MM, Ammar SH, Taher AG (2024) Decoration of 0D Bi_3NbO_7 nanoparticles onto 2D $BiOIO_3$ nanosheets as visible-light responsive S-scheme photocatalyst for photo-oxidation of antibiotics in wastewater. Environ Res 243: 117854.

40. Gao X, Li B, Jian S (2022) Step-scheme $CeO_2/CaIn_2S_4$ heterostructured photocatalysts for efficient reduction of Cr (VI) under visible light. Colloids Surfaces A Physicochem Eng Asp 648: 129168.

41. Jabbar ZH, Graimed BH, Ammar SH, Taofeeq H, Alsunbuli MMB, et al. (2024) A critical review describes wastewater photocatalytic detoxification over Bi_5O_7I-based heterojunction photocatalysts: characterizations, mechanism insight, and DFT calculations. J Environ Chem Eng 12(2): 112241.

42. Jabbar ZH, Graimed BH, Alsunbuli MM, Sabit DA (2023) Developing a magnetic bismuth-based quaternary semiconductor boosted by plasmonic action for photocatalytic detoxification of Cr(VI) and norfloxacin antibiotic under simulated solar irradiation: Synergistic work and radical mechanism. J Alloys Compd 958: 170521.

43. Li J, Meng S, Wang T, Xu Q, Shao L, et al. (2017) Novel $Au/CaIn_2S_4$ nanocomposites with plasmon-enhanced photocatalytic performance under visible light irradiation. Appl Surf Sci 396: 430-437.

44. Wang L, Wan Z, Xu X, Qian J (2023) $CaIn_2S_4$–In_2O_3 hybrid nanofibers with expedited photocarrier separation for fast photocatalytic bacterial inactivation under visible light. Inorg Chem Front 10(5): 1650-1659.

45. Gao X, Jian S, Wang W, Li B, Huang J, et al. (2023) Study on Photochemical Properties of a $Sr\text{-}SnS_2/CaIn_2S_4$ Heterostructure to Improve Cr(VI) Removal. Langmuir 39(30): 10542-10552.